

Interpenetration and Friction of Brush-Coated Surfaces under External Load: Analytical Theory and SCF Calculations

Leonid I. Klushin,* Anna S. Ivanova, Alexey A. Polotsky, and Alexander M. Skvortsov



Cite This: *Macromolecules* 2023, 56, 5188–5200



Read Online

ACCESS |



Metrics & More

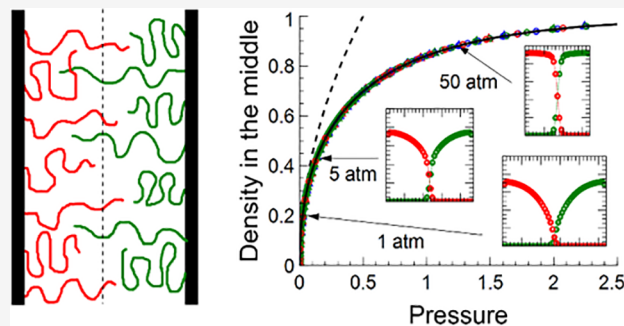


Article Recommendations



Supporting Information

ABSTRACT: We studied the compression and interpenetration properties of two opposing monodisperse polymer brushes under external load by analytical theory and by a numerical self-consistent field (SCF) approach. Analytical expressions are proposed for the brush density profiles in the interpenetration zone and verified by numerical SCF calculations. We quantify the interpenetration of two opposing brushes by the characteristic penetration length and by two integral parameters: the overlap integral, Γ , representing the number of interbrush contacts, and the number of brush monomer units in the foreign half-space, Σ . The interpenetration parameters are studied in two conjugate ensembles as functions of the brush separation and of the external pressure. We propose a theoretical description of the solvent-mediated friction force in the low shearing rate regime on the basis of the Brinkman equation for two compressed brushes sliding against each other. We demonstrate that the total friction force which also includes direct brush–brush friction is expressed in terms of Γ and Σ . The SCF data for the interpenetration parameters Γ and Σ and hence for the total sliding friction force in the pressure ensemble collapse onto universal master curves when rescaled by the factor $(N/\sigma)^{1/3}$ as suggested by the theory, where N is the chain length and σ is the surface grafting density. Finally, we define the kinetic friction coefficient as a function of the external pressure and analyze its universal rescaled behavior in the two limits of nondraining and free-draining brushes.



1. INTRODUCTION

Polymer brushes are commonly used for permanent surface modification to mediate the stability of colloidal dispersions, provide antifouling properties, and protect the system from degradation.¹ Brushes can also act as smart stimuli-responsive materials that change surface wetting properties reversibly or act as sensors.^{2,3} Interactions between surfaces modified by tethered polymer layers are multifaceted and include both equilibrium and dynamic phenomena. They play an important role in various fields. For example, they mediate the stability of colloidal dispersions, prevent direct contact between surfaces, protect the system from degradation, modify friction forces between the surfaces, and have important applications as lubricants in machine parts and artificial joints.^{4–6} The compression force and the interpenetration of brushes have been the subject of numerous publications, including experimental,^{4,5,7–9} theoretical,^{10–12} and computational work^{13–18} (see also a recent review¹⁹). The physical properties of isolated brushes under good solvent conditions are determined by two key parameters: the chain length and the grafting density. Together they define the thickness of the brush layer and the strength of the repulsive forces that the brush exerts on objects approaching the surface.

As two brushes are brought into contact, two processes are found to occur concurrently: interpenetration and compression. When the distance D between the brushes equals twice

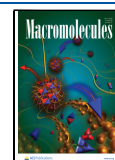
the maximum extent of each, the parabolic profiles of both brushes start overlapping and the density increases everywhere between the two grafting surfaces. At small separations the overall density becomes almost uniform in the gap between the grafting surfaces. Several parameters were proposed in order to quantify the amount of interpenetration.

Traditionally, all theoretical work as well as simulations of brush compression and interpenetration were set in the constant separation ensemble, i.e., the brush separation D was taken as the control parameter. Often simulations will investigate confined brushes without explicit solvent,^{20,21} as this both simplifies and speeds up the simulations. The curves of the normal pressure vs separation distance were calculated in ref 22 and analyzed in conjunction with the density profiles at each distance to determine the structure–property relationships. Some simulations have included explicit solvent but maintained a constant total number density upon compression, not exactly reproducing experimental conditions.^{14,23} In the

Received: March 13, 2023

Revised: May 15, 2023

Published: June 16, 2023



work by Goujon et al.,^{24,25} DPD simulations included explicit solvent with the chemical potential imposed by the solvent reservoir which also indirectly controlled the solvent pressure.

The ensemble in which the separation distance, D , plays the role of the control variable (Helmholtz NVT ensemble) does not necessarily reflect typical experimental settings. Even in carefully controlled experiments with surface force apparatus maintaining a fixed distance is quite difficult. The situation is dramatically different when natural objects are concerned: the separation between brush-coated surfaces will be invariably adjusted depending on the applied external pressure. It is therefore only natural to recast the discussion of interpenetration into the language of the Gibbs NPT ensemble with the external pressure as the independent variable. A comparison of tribological properties of different pairs of brush-coated surfaces also looks much more natural under the condition of the same applied normal pressure supplied by external loading. We identify the pressure due to external loading with the osmotic pressure Π since in a typical experimental setting the solvent permeating the brushes is connected to a reservoir exposed to atmospheric pressure which is also transmitted to the exterior of the brush-coated surfaces. Our ultimate goal is to describe the sliding friction force as a function of the external load and to identify the role of the brush parameters in defining the friction coefficient which may be also pressure dependent.

The paper is organized as follows. Section 2 describes the implementation of the numerical SCF model within the Scheutjens–Fleer formulation. In section 3 A, we summarize the main results on the compression and interpenetration of two opposing monodisperse brushes immersed in good solvent and establish an approximate analytical mapping between the two ensembles on the basis of the equation of state for semidilute solutions applied to the segment density at the midplane. In section 3 B, we establish a connection between two integral interpenetration parameters and the contributions to the net friction force due to brush–brush and brush–solvent friction. In order to evaluate the latter, we extend the Brinkman equation approach to the situation when two interpenetrating brushes are sliding against each other. Section 3 C explores the penetration length, the integral interpenetration parameters, and the friction coefficients in the pressure ensemble and verifies the collapse of the data points onto universal master curves after rescaling as suggested by the analytical theory. Section 4 presents a summary of the main results.

2. MODEL AND METHOD

We consider a monodisperse polymer brush made of linear flexible macromolecules grafted at one end onto a solid planar substrate. A polymer chain is composed of N identical monomer units; the chains are grafted onto the surface at the grafting density σ , defined as the number of grafted polymer chains per unit surface area. The brush is immersed into an athermal solvent; in terms of Flory–Huggins interaction parameter χ , this corresponds to $\chi = 0$.

To calculate the system's partition function and its various properties, we use the Scheutjens–Fleer self-consistent field (SF-SCF) method. The SF-SCF method and its modifications for the study of polymer brushes of various types have been repeatedly described in the literature and can be found in refs 26–28. The SF-SCF approach uses a lattice and also takes into account the geometry and the symmetry of the problem under

consideration. For the planar polymer brushes, the choice of the simple cubic lattice is obvious; polymer chains are modeled as walks on this lattice. The lattice cell size is equal to the size of a monomer unit a , and each lattice site can be occupied either by a monomer unit or by a solvent molecule. The lattice sites are organized in planar layers; each layer is referred to with a coordinate z normal to the grafting plane. Within a layer with fixed z , i.e., along x and y axes, the volume fractions of the monomeric components and the self-consistent potential are taken as uniform; hence, we use a one-gradient version of the SF-SCF method for planar geometry.

Details of the implementation of the SF-SCF for two opposing interacting polymer brushes can be found in the Appendix of ref 29. SF-SCF calculations were performed by using the sbox program developed in the Laboratory of Physical and Colloid Chemistry at the University of Wageningen (The Netherlands). Throughout this paper we will use the monomer unit size $a = 1$ as the unit length and $k_B T = 1$ as the energy unit.

3. RESULTS

3.1. Normal Pressure and Interpenetration of Two Opposing Brushes in the D Ensemble (Fixed Separation). Traditionally, the normal pressure in the brush due to compression is calculated from the derivative of the total free energy A_{tot} of the opposing brushes system per unit area with respect to the separation D between the grafting surfaces: $\Pi(D) = -\frac{\partial A_{\text{tot}}}{\partial D}$. The earliest approach is based on the Alexander box-like brush model where all chains have the same length, N , and the same normal end-to-end distance, as if the free ends of the brush chain were attached to a virtual second planar plate. The free energy can be written in the mean-field approximation³⁰ including the density-dependent interaction contribution and the elastic free energy due to chain stretching or on the basis of the scaling blob picture,³¹ providing a prediction for the normal pressure as a function of the brush separation, $\Pi(D)$. This model underestimates the brush thickness and compares only qualitatively to simulations and experiments. A more sophisticated theory by Milner, Witten, and Cates³² takes into account the possibility that the nongrafted chain ends may be located anywhere in the brush. Within the SCF framework in the strong stretching approximation and employing the interaction free energy density in the second virial form, one obtains a parabolic (rather than a step-like) density profile. The total free energy of the opposing brush system was also evaluated by ref 32 as a function of separation, D , and the resulting normal pressure produced by differentiation can be cast into the following form

$$\Pi(D) = \frac{\nu}{2} \left(\frac{N\sigma}{H_0} \right)^2 \left[\frac{2H_0}{D} - \left(\frac{D}{2H_0} \right)^2 \right]^2 \quad (1)$$

where

$$H_0 = \left(\frac{2}{\pi} \right)^{2/3} (\sigma\nu/a)^{1/3} Na \quad (2)$$

is the unperturbed brush height, ν is the excluded volume parameter, N is the chain length, σ is the surface grafting density, and a is the segment length which is taken as a unit length hereafter. Since most of the effects under investigation are of entropic nature, the energy unit is $k_B T$, where T is the

temperature and k_B is the Boltzmann constant. In our earlier paper³³ we proposed an alternative approach for calculating the normal pressure by linking it to the monomer density at the midplane between the brushes via the equation of state. A representative picture of the individual brush density profiles, $\varphi_1(z)$ and $\varphi_2(z)$, in a system of two compressed interpenetrating brushes is displayed in Figure 1. The total

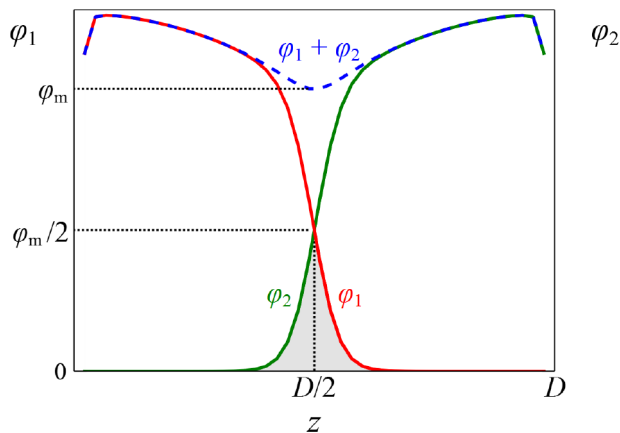


Figure 1. Individual brush density profiles $\varphi_1(z)$ and $\varphi_2(z)$ and the overall density profile, $\varphi_1(z) + \varphi_2(z)$, for a pair of compressed opposing brushes separated by the distance D . The shaded area represents the interpenetration zone. φ_m is the total polymer density at the midplane located at the distance $z = D/2$.

monomer density profile is also shown. It is clear that due to symmetry the total density at the midplane, φ_m , includes two equal contributions $\varphi_1(D/2) = \varphi_2(D/2) = \varphi_m/2$.

From the point of view of the analytical theory, evaluation of the midplane density for two opposing monodisperse brushes is based on the assumption that brush interpenetration does not affect the pressure: one can imagine that both brushes meet at $z = D/2$, an impenetrable midplane with $\varphi_1(D/2 - 0) = \varphi_2(D/2 + 0) = \varphi_m$. Within the strong-stretching approximation,³² the density profile of a brush compressed by an impenetrable wall remains parabolic with the same curvature but is uniformly shifted upward according to the compression distance. Direct implementation of this idea gives the monomer density at the midplane as

$$\varphi_m = \frac{N\sigma}{H_0} \left[\frac{2H_0}{D} - \left(\frac{D}{2H_0} \right)^2 \right] \quad (3)$$

The interaction free energy per unit volume makes no distinction between a semidilute polymer solution and some region in the brush interior and is completely defined by the local monomer density, φ . Within the second virial approximation is a simple quadratic form $A_{\text{vir}} = \frac{\nu}{2}\varphi^2$. The osmotic pressure as a function of the local monomer density (i.e., the equation of state for a semidilute polymer solution) is generated by the Legendre transform of the free energy density and within the second virial approximation coincides with it

$$\Pi_{\text{vir}}(\varphi) = \varphi \frac{\partial A_{\text{vir}}}{\partial \varphi} - A_{\text{vir}} = \frac{\nu}{2}\varphi^2 \quad (4)$$

Direct examination of eqs 1, 3, and 4 shows that the calculation based on the total free energy of compressed brushes, eq 1, is immediately reproduced if one applies the equation of state in

the second virial form to the central density: $\Pi(D) = \Pi_{\text{vir}}(\varphi_m(D))$.

The equivalence of the approaches based on differentiating the total free energy with respect to the brush separation and on applying the equation of state to the monomer density at the midplane was verified numerically for both monodisperse and polydisperse brushes³³ where the virial equation of state in eq 4 was implemented in the MC scheme at the level of the microscopic Hamiltonian. From a general point of view, this equivalence can be understood as follows: The derivative of the free energy is linked to the isothermal work of moving the grafting plane of one of the brushes; therefore, it is related to the applied external pressure. At mechanical equilibrium, the normal pressure must be uniform across the bilayer. At each cross-section at the position z , it has two contributions: one (isotropic) related to the average local density by the equation of state and the other (anisotropic) due to the tension in the brush-forming chains. The latter term is negative and concerns only the normal direction. At the midplane, the total density profile passes through a minimum, which means that the gradient of the chemical potential is zero, and the local chain tension at this position vanishes as well. Hence, the total pressure is reduced to the density-dependent term representing the equation of state and is expected to be completely isotropic. The above considerations are quite general and not restricted to the specific form of the equation of state. In the present work, the equation of state is derived from the Flory–Huggins free energy density expression for a semidilute polymer solution

$$A_{\text{FH}}(\varphi) = (1 - \varphi)\log(1 - \varphi) + \chi\varphi(1 - \varphi) \quad (5)$$

where χ is the Flory–Huggins parameter. The pressure, $\Pi_{\text{FH}} = \varphi \frac{\partial A_{\text{FH}}}{\partial \varphi} - A_{\text{FH}}$, is given by

$$\Pi_{\text{FH}}(\varphi) = -\varphi - \log(1 - \varphi) - 2\chi\varphi^2 \quad (6)$$

At small densities, the pressure is still dominated by the second virial term, eq 4, where the excluded volume parameter is given by $\nu = 1 - 2\chi$. In the following, we focus on the athermal solvent with $\chi = 0$ and $\nu = 1$.

We demonstrate the equivalence of the two approaches described above to pressure in brushes described by the Flory–Huggins free energy density in Figure 2, displaying the osmotic pressure as a function of the separation between the two planar brush-coated surfaces.

The main goal of the present paper is to establish a relation between the normal osmotic pressure and the lateral friction forces generated by shearing. Within this line of reasoning, interpenetration of brushes plays a central role.

In order to quantify the brush interpenetration we employ several different parameters. Historically, the first one was introduced by Murat and Grest in their pioneering work³⁴ and has the meaning of the fraction of the brush monomers residing in the foreign half-space (beyond the midplane)

$$I = \frac{\int_{D/2}^D \varphi_1(z) dz}{\int_0^D \varphi_1(z) dz} = \frac{\int_{D/2}^D \varphi_1(z) dz}{N\sigma} \quad (7)$$

where $\varphi_1(z)$ is the monomer density profile due to the left brush only. A closely related parameter is the non-normalized integral

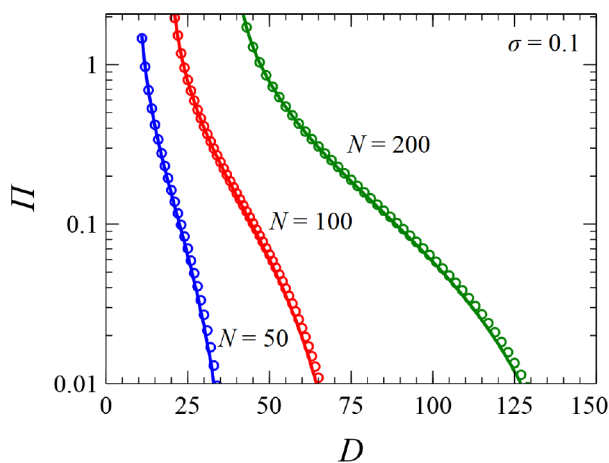


Figure 2. Normal osmotic pressure as a function of the brush separation D : comparing the calculation by equation of state, eq 6, applied to the monomer density at the midplane, $\Pi(D) = \Pi_{\text{FH}}(\varphi(D/2))$ (solid lines) and by differentiating the total free energy of the compressed brush system $\Pi(D) = -\frac{\partial A_{\text{tot}}}{\partial D}$ (points); brush parameters are indicated in the figure.

$$\Sigma = \int_{D/2}^D \varphi_1(z) dz \quad (8)$$

which has the meaning of the number of monomers (per unit area) belonging to one of the brushes and residing beyond the midplane and is graphically represented by one-half of the dashed area in Figure 1. We demonstrate below that this parameter is directly involved in the lateral friction force resulting from brush–solvent interactions. The third important parameter describing the brush interpenetration is the overlap integral Γ . It is based on the overlap function defined as the product of the two individual density profiles, $\varphi_1(z)\varphi_2(z)$, which gives the local probability density of interbrush contacts in the mean-field approximation neglecting the density–density correlations between the two brushes.¹⁷ The overlap integral

$$\Gamma = \int_0^D \varphi_1(z)\varphi_2(z) dz \quad (9)$$

is thus a measure of the number of interbrush contacts per unit area. We demonstrate later that parameters Σ and Γ are directly involved in the lateral friction force resulting from brush–solvent and brush–brush interactions.

The overlap function was approximated in ref 17 by a Gaussian function $\varphi_1(z)\varphi_2(z) \approx \exp\left[-\left(\frac{z/D-1/2}{\delta}\right)^2\right]$, where δ had the meaning of the characteristic penetration length expressed as a fraction of the separation and was extracted as a fitting parameter. A more consistent expression for the overlap function was proposed in our earlier work¹² based on the observation that the individual brush density profiles have exponentially decreasing tails and an inflection point at the midplane $z = D/2$ where $\varphi_1(z) = \varphi_2(z) = \frac{\varphi_m}{2}$ (see also Figure 1). This leads to an Ansatz

$$\varphi_{1,2}(z) = \frac{\varphi_m}{2} \left[1 \mp \tanh\left(\frac{z - D/2}{\delta}\right) \right] \quad (10)$$

where δ naturally defines the characteristic penetration length. The Ansatz is tested in Figure 3a, which shows a very good correspondence between the results of the numerical SCF calculations and the theory assumption. We note that while outside the interpenetration zone individual brush density profiles may still have approximately parabolic shapes deviating from eq 10, this is of no significance for the integral interpenetration parameters Σ and Γ as their definitions attest. It follows that the overlap function must have the form

$$\varphi_1(z)\varphi_2(z) = \frac{\varphi_m^2}{4} \cosh^{-2}\left(\frac{z - D/2}{\delta}\right) \quad (11)$$

which is very well supported by numerical SCF calculations, see Figure 3.

The analytical Ansatz, eq 10, leads to very simple relations between the total density at the midplane φ_m , the penetration length δ , and the interpenetration parameters Γ and Σ defined above

$$\Gamma = \delta \frac{\varphi_m^2}{2} \quad (12)$$

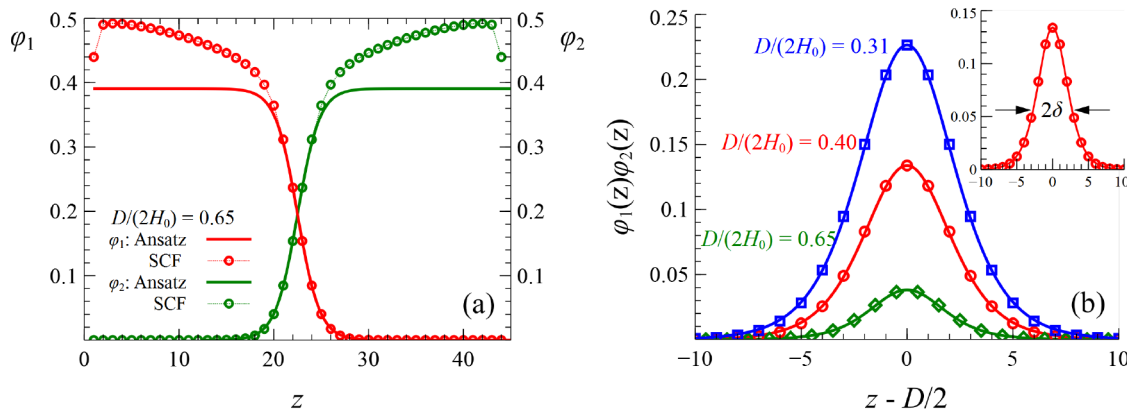


Figure 3. (a) Comparison of individual density profiles of compressed opposing brushes, $\varphi_1(z)$ and $\varphi_2(z)$ (symbols connected by thin lines to guide the eye), and their approximations by eq 10 calculated at $\delta = 2.34$. (b) The overlap function $\varphi_1(z)\varphi_2(z)$ obtained by SCF calculations (symbols) compared to the theoretical Ansatz, eq 11 (lines), for compressed opposing brushes at different degrees of compression $D/(2H_0) = 0.65$ (diamonds, green), 0.40 (circles, red), and 0.31 (squares, blue). Brush parameters are $\sigma = 0.1$ and $N = 100$. (Inset) Width of the overlap function at the level of $\cosh^{-2}(1) \approx 0.42$ of the maximum.

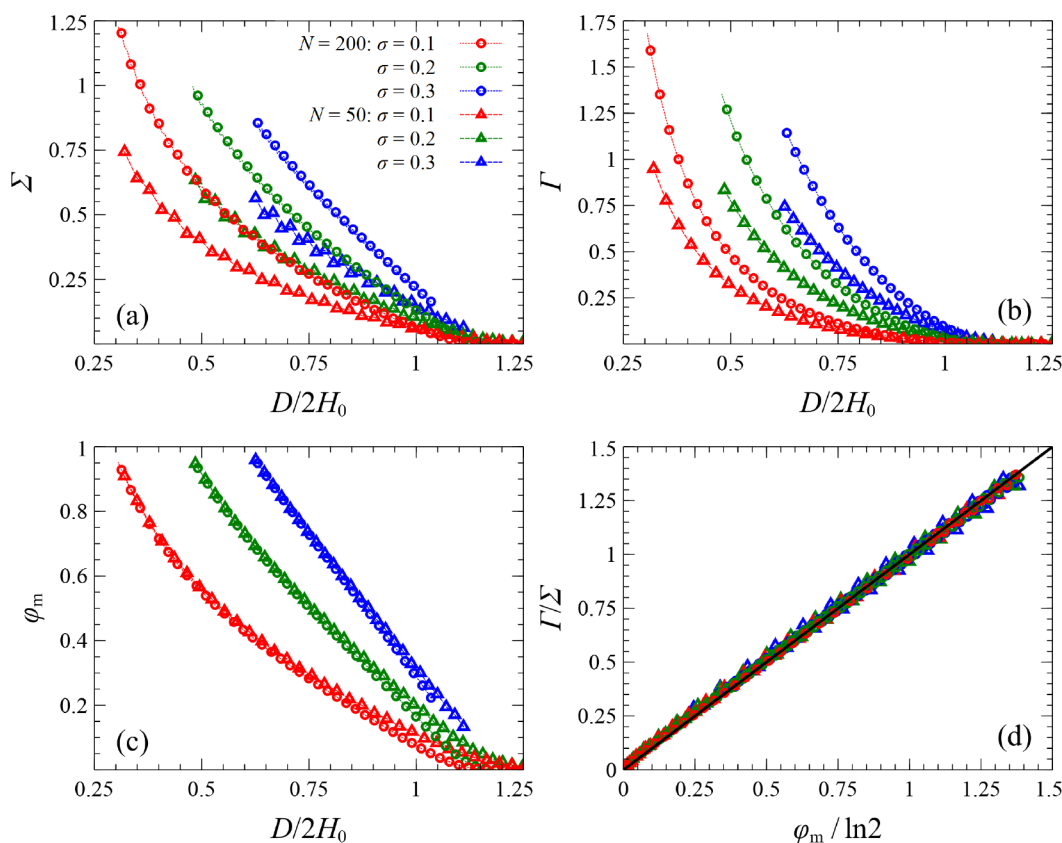


Figure 4. Number Σ of monomer units per unit area belonging to one of the brushes and residing in the foreign half-space (beyond the midplane) (a), overlap integral Γ (b), and monomer density at the midplane ϕ_m (c) as functions of the reduced brush separation $D/(2H_0)$. Chain length N and grafting density σ are indicated in panel a. The data are obtained by numerical SCF calculations and are shown by symbols. (d) Ratio Γ/Σ vs $\frac{\phi_m}{\ln 2}$ predicted to be a linear function with a unit slope, eq 15.

$$\Sigma = \delta \cdot \frac{\phi_m}{2} \cdot \ln 2 \quad (13)$$

$$I = (N\sigma)^{-1} \Sigma \quad (14)$$

Here, it was assumed that the separation distance D is much larger than the interpenetration zone so that the appropriate integration limits can be extended to infinity.

Interpenetration parameters Σ and Γ together with the midplane density ϕ_m are shown in Figure 4a–c as functions of relative separation, $D/2H_0$, for brushes with different chain lengths and grafting densities. There is no obvious universality in the curves presented. The theory predicts, however, that the ratio

$$\Gamma/\Sigma = \frac{\phi_m}{\ln 2} \quad (15)$$

is independent of the brush parameters when considered as a function of the midplane density. Figure 4d tests this prediction whereby all of the data points collapse on a single straight line with the unit slope. In view of the discussion of the normal pressure being completely defined by the midplane density, we expect the ratio Γ/Σ to be a universal function of the normal pressure for all brushes independently of what their parameters are.

3.1.1. Scaling Relation for the Penetration Length. A scaling argument for the penetration length as a function of the separation between brush-coated surfaces was originally proposed by Wittten et al.³⁵ and is based on simple

considerations.^{5,33} The effective potential imposed by the opposing brush in the interpenetration zone is counted from the reference position at the midplane and approximated by the linear term of the Taylor expansion: $U(z) = (D/2 - z) \frac{dU}{dz} \Big|_{z=D/2}$. The analytical SCF theory in the strong-stretching approximation asserts that the effective potential profile of a compressed brush still has a parabolic form $U(z) = \text{const} - \frac{3\pi^2 z^2}{8N^2}$, and hence the relevant slope (absolute value) is $\frac{dU}{dz} \Big|_{z=D/2} = \frac{3\pi^2 D}{8N^2}$. The free energy cost for placing a tail consisting of n monomers in the foreign region within distance δ from the midplane is estimated (up to coefficients of order 1) as $\Delta A \approx n\delta \frac{dU}{dz}$. Taking $\Delta A \approx 1$ and assuming that the tail conformation is a weakly perturbed ideal coil with $n \approx \delta^2$ one arrives at

$$\delta \approx \left(\frac{dU}{dz} \right)^{-1/3} = B \left(\frac{3\pi^2 D}{8N^2} \right)^{-1/3} \quad (16)$$

where B is a numerical prefactor to be determined by comparing the scaling prediction to the results of the numerical SCF calculations where the penetration length is extracted from the integral interpenetration parameters according to eqs 12 and 13. Figure 5 shows the comparison when the prefactor value is identified as $B = 0.58$.

$$\delta = B \frac{2}{3^{1/3} \pi^{2/3}} D^{-1/3} N^{2/3} \simeq 0.38 D^{-1/3} N^{2/3} \quad (17)$$

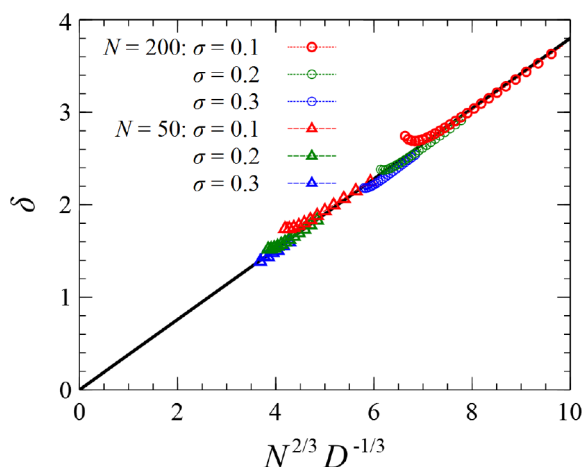


Figure 5. Penetration length in the D ensemble: scaling prediction (line) compared to the numerical SCF results (symbol). The fitting prefactor in eq 17 is taken as $B = 0.58$.

Most of the SCF data fits the predicted scaling very well. Some deviations appear when the brush separation is such that the brushes just barely touch each other. The actual brush density profile at the outer edge has a nonparabolic diffuse tail with low slope which is not accounted for by the analytical theory in the strong-stretching approximation but results in an increased penetration length.

3.2. Connection of the Interpenetration Parameters to Shearing Friction Forces. The two interpenetration parameters are not just some equilibrium characteristics of the opposing brush system. According to the linear response theory, they must be linked to dissipation when shearing stress is applied and the brushes slide against each other at some stationary velocity V . Different regimes of the brush response to the shearing deformation are controlled by the Weissenberg number, Wi , which is defined as a product of the brush chain relaxation time and the typical shearing rate $Wi = \tau\dot{\gamma}$. Although simulations clearly show that under shearing deformation the brush chains acquire slanted conformations, at low shearing rates with $Wi \leq 0.3$, lateral stretching is decoupled from the brush chain behavior along the normal direction,¹⁶ and hence, hydrodynamic parameters can be linked to equilibrium brush characteristics in the absence of shear. At larger Weissenberg numbers $Wi \gtrsim 1$, coupling between normal and lateral deformations becomes important. It was demonstrated by MD simulations that the overlap integral Γ essentially defines the friction force appearing when two dry brushes are sheared against each other.^{18,25,36} A natural assumption for low sliding velocities is formulated as follows

$$F_{bb} = \zeta_{bb} \Gamma V \quad (18)$$

where F_{bb} is the friction force per unit area due to brush–brush contacts, V is the velocity of one brush with respect to another, Γ is the average number of interbrush contacts per unit area, and the proportionality coefficient ζ_{bb} has the meaning of the viscous friction coefficient per one brush–brush contact. If the brushes are immersed in a solvent, one would expect additional dissipation due to the relative motion of brushes against the solvent.

The considerations above suggest that the two interpenetration parameters under our scrutiny have direct bearing on the tribological characteristics of the compressed opposing brushes.

3.2.1. Brinkman Equation and Brush–Solvent Friction. Here, we propose a more rigorous approach to evaluate the sliding friction forces mediated by the induced solvent flow within the two moving interpenetrating brushes. Detailed understanding of the flow-mediated forces is quite challenging and requires either approaches based on system-specific versions of complex fluids hydrodynamics or explicit dynamic simulations. Simulations turned out to be very important in clarifying the flow-related behavior for which conflicting theoretical predictions had been proposed, e.g., flow-induced swelling or flattening of brushes. We address the questions of the solvent velocity profile within the pair of sliding interpenetrating brushes and the resulting friction forces following the approach of Milner¹⁰ (see also ref 12), who evaluated the hydrodynamic penetration depth for a single monodisperse brush by assuming that the unperturbed brush density profile can be described by position-varying screening length $\lambda(x)$ introduced in the seminal paper by Brinkman.³⁷ In a single brush subject to tangential shear flow under stationary conditions and in the absence of pressure gradients, the equation describing the tangential velocity component, u , as a function of the normal coordinate, z , reads

$$\frac{d^2 u}{dz^2} = \lambda^{-2}(z) u \quad (19)$$

The position-dependent prefactor, $\lambda^{-2}(z)$, is also referred to as the inverse permeability, $\kappa(z)$, and in the polymer brush context must be linked to the local monomer density $\varphi(z)$. The right-hand side of eq 19 has direct physical meaning: when multiplied by the solvent viscosity, η , it represents the negative of the volume density of the lateral friction force applied by the immobile porous medium on the solvent flow.

3.2.2. Brush–Solvent Friction from Brinkman Equation for Two Sliding Brushes. We extend the Brinkman equation approach to the situation when there are two interpenetrating brushes, one stationary and the other moving at a constant tangential velocity V . Then, the net force applied to the flow locally has two contributions

$$\frac{d^2 u}{dz^2} = \kappa_1(z) u + \kappa_2(z) (u - V) \quad (20)$$

The first term is proportional to the flow velocity with respect to the stationary brush, while the second term is proportional to the velocity of the flow with respect to the moving brush. The influence of two opposing brushes is characterized by the two inverse permeability profiles $\kappa_1(z)$ and $\kappa_2(z)$, respectively. The solution of eq 20 subject to the boundary conditions $u(0) = 0$ and $u(D) = V$ defines the solvent velocity profile that we expect to be a smoothed step function. Away from the interpenetration zone only one term in eq 20 survives, and the flow velocity quickly reaches the limits $u \rightarrow 0$ inside the first brush and $u \rightarrow V$ inside the second brush. By symmetry, one expects the flow velocity at the midplane to be $u(D/2) = V/2$. In order to understand the width of the smoothed step profile, one must keep in mind that two characteristic length scales are involved: the hydrodynamic correlation length λ most importantly related to the combined inverse permeability $\lambda^{-2} = \kappa_1(D/2) + \kappa_2(D/2)$ at the midplane and linked to the total

monomer density there and the interpenetration length δ which controls the shape of the individual brush profiles in the interpenetration zone and appears explicitly in the inhomogeneous term $-\kappa_2(z)V$. The inverse permeability profiles in the interpenetration zone must also be controlled by the penetration length. The exact shape of the functions $\kappa_{1,2}(z)$ depends on the assumption made about the connection between the permeability and the local brush density and is discussed in more detail in the [Supporting Information](#).

It is clear that the hydrodynamic length decreases with the increasing central density and hence at very large pressures must go down to one monomer length. Moreover, at any finite central density, the hydrodynamic length is defined locally and therefore is independent of the brush chain length. On the other hand, the interpenetration length is proportional to $N^{1/3}$ and, moreover, grows with compression. Hence, the regime defined by the strong inequality $\delta \gg \lambda$ always exists under the conditions of moderate to strong compression for brushes made of long chains. In this limit, an approximate analytical solution of [eq 20](#) can be written within a perturbation-like approach (see the [Supporting Information](#)).

The approximate solution has the form

$$u_0(z) = \frac{\kappa_2(z)}{\kappa_1(z) + \kappa_2(z)}V \quad (21)$$

We use the approximate solvent velocity profile to obtain a simple estimate for the friction force contribution due to the brush interacting with the solvent flow. By the Newton's third law, the force per unit volume acting on the first brush by the flow has the form

$$f \simeq \eta \kappa_1(z) u_0(z) = \frac{\kappa_2(z) \kappa_1(z)}{\kappa_1(z) + \kappa_2(z)}V \quad (22)$$

and the net force per unit area due to the brush–solvent friction is obtained by integration

$$F_{\text{bs}} = \eta V \int_0^D \frac{\kappa_2(z) \kappa_1(z)}{\kappa_1(z) + \kappa_2(z)} dz \quad (23)$$

where η is the solvent viscosity. Several versions were proposed for the connection between the inverse permeabilities $\kappa_{1,2}(z)$ and the respective brush density profiles $\varphi_{1,2}(z)$ as discussed in the [Supporting Information](#). We explicitly consider the nondraining limit following [ref 10](#) and the draining limit studied by [Suo et al. et al.³⁸](#) The result for the brush–solvent friction force is given by

$$F_{\text{bs}} = \begin{cases} \frac{\pi - 2}{4} \eta V \Gamma & \text{nondraining} \\ \eta V \left(\frac{\Sigma}{\ln 2} + \frac{\Gamma}{2} \right) & \text{free draining} \end{cases} \quad (24)$$

Simulations by dissipative particle dynamics method³⁹ can be used to check the validity of theories that describe the solvent flow, such as the Brinkman equation and, in particular, the dependence of the position-dependent screening length on the local monomer density. According to these simulations for rather short brush chains with $N = 20$, for several grafting densities the data on the screening length λ as a function of the monomer density collapse onto a master curve giving $\lambda \approx \varphi^{-0.55}$. This is in better agreement with the free-draining

treatment as opposed to the nondraining relation in the in the mean-field approximation $\lambda \approx \varphi^{-1}$ utilized in [ref 10](#).

3.2.3. Net Friction Force. We combine the [eq 18](#) for the brush–brush friction force with the two limiting expressions for the brush–solvent friction force, [eq 24](#), and note that the product ηa , where a is the (unit) segment length, has the meaning of a Stokesian friction coefficient ζ_{bs} per monomer. Hence, in the nondraining limit, the net friction force turns out to be entirely determined by the overlap integral

$$F_{\text{fr}} = V \left(\zeta_{\text{bb}} + \zeta_{\text{bs}} \frac{\pi - 2}{4} \right) \Gamma \quad (25)$$

In the free-draining limit as discussed in [ref 38](#), the total friction force has two contributions proportional to the two interpenetration parameters Σ and Γ

$$F_{\text{fr}} = V \left[\left(\zeta_{\text{bb}} + \frac{\zeta_{\text{bs}}}{2} \right) \Gamma + \frac{\zeta_{\text{bs}}}{\ln 2} \Sigma \right] \quad (26)$$

3.3. Pressure Ensemble. Historically, theoretical work as well as simulations of compression and interpenetration of opposing brushes employed the brush separation as the control variable. We have argued in the [Introduction](#) that recasting the study of interpenetration in the language of the pressure ensemble makes good sense. Comparing the tribological properties of different brush-coated surfaces also looks much more natural under the condition of the same applied normal pressure (external loading). We identify the pressure due to external loading with the osmotic brush pressure Π since in a typical experimental setting the solvent permeating the brushes is connected to a reservoir exposed to atmospheric pressure. The same atmospheric pressure is transmitted to the exterior of the brush-coated surfaces so that the external load is balanced solely by the osmotic brush pressure.

The relation between the ensemble with fixed distance (D ensemble) and the ensemble with fixed externally applied pressure (Π ensemble) is established by expressing the pressure as a function of the brush separation and was traditionally done through the derivative of the total free energy of compression (per unit area) with respect to the distance, $\Pi(D) = \frac{\partial A_{\text{tot}}}{\partial D}$. A more direct alternative connection is provided by the equation of state applied to the midplane density, $\Pi(D) = \Pi(\varphi_{\text{m}}(D))$, as discussed above.

In the pressure ensemble, we treat the monomer density at the midplane as a function of the applied pressure (as the independent variable) which is given by the inverse of [eq 6](#) with $\chi = 0$ and is displayed in [Figure 6](#). Profiles in the inset illustrate the relevant interpenetration profiles corresponding to three different values of the pressure applied. In order to relate the illustrations to the everyday life pressure scale, we recall that the natural unit of the osmotic pressure is $\frac{k_{\text{B}}T}{a^3}$, where k_{B} is the Boltzmann constant, T is the temperature, and a is the Kuhn segment length. Taking $T = 300$ K and $a = 1$ nm, we get an estimate of the natural unit of pressure $\Pi = 1$ to be close to 40 atm. Insets show illustrative interpenetration profiles corresponding to three different values of the pressure applied: panels in [Figure 6](#) correspond to 1 (the most common everyday value), 5, and ≈ 50 atm. The last value corresponds to the maximum pressure at which brush-coated artificial joints operate.⁶ Note that the pressure range less than 5 atm is well described by the equation of state in the second virial approximation.

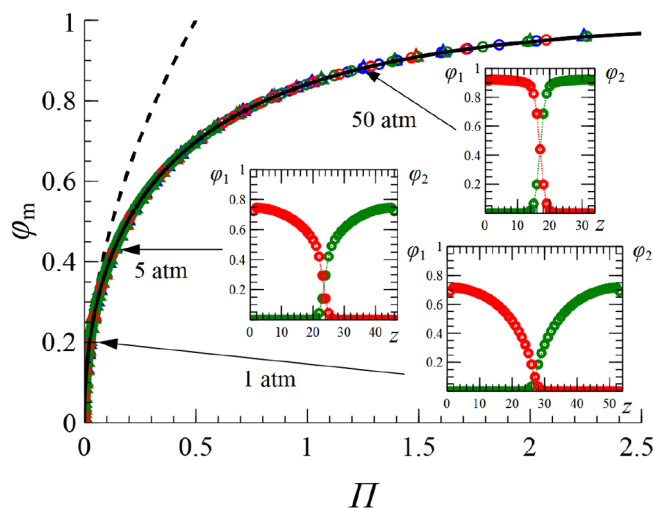


Figure 6. Monomer density at the midplane between two compressed opposing brushes as a function of the applied pressure. Symbols are SCF calculation results (the pressure is calculated by differentiating the total free energy of the compressed brushes), solid line represents the equation of state (6) with $\chi = 0$, dashed line corresponds to the equation of state (eq 4) in the second virial approximation. The legend for the data points is the same as that in Figure 5. (Insets) Representative density profiles for three different pressures, as indicated in the figure.

Examining eqs 12 and 13 for the two interpenetration parameters of interest we note that since ϕ_m is uniquely defined by the applied external pressure, all of the effects of the brush parameters (chain length, grafting density, and even polydispersity which we do not discuss here) on the overlap integral, Γ , and on the number of monomers in the foreign half-space, Σ , are encoded in the penetration length $\delta(\Pi; N, \sigma)$ which is to be treated now as a function of the external pressure Π as the independent variable, and of the brush parameters.

To make a connection between the penetration length, the pressure, and the brush parameters, we recast eq 17 in terms of the relative deformation, $\frac{D}{2H_0}$:

$$\begin{aligned} \delta &= A \left(\frac{2}{\pi} \right)^{4/9} 2^{-1/3} \sigma^{-1/9} \left(\frac{D}{2H_0} \right)^{-1/3} N^{1/3} \\ &= 0.383 \sigma \left(\frac{D}{2H_0} \right)^{-1/3} N^{1/3} \end{aligned} \quad (27)$$

This, in turn, is uniquely defined by the density at midplane by eq 3, which can be recognized as a cubic equation for $x = D/(2H_0)$

$$x^3 + \phi_m \left(\frac{\pi\sigma}{2} \right)^{-2/3} x - 1 = 0 \quad (28)$$

the real root of which gives $\frac{D}{2H_0}(\phi_m)$. The general Cardano's expression for the root is cumbersome and not easily tractable; however, it is perfectly useful for analytical calculations of the penetration length as a function of the applied pressure according to eqs 27, 28, and 6. Figure 7 shows the numerical SCF data in comparison with the analytical predictions.

Three important features of the penetration length behavior are worth noting. (i) The penetration length is generally a

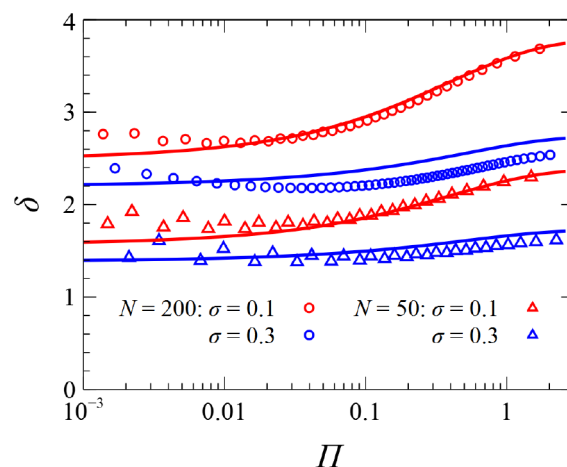


Figure 7. Penetration length as a function of the applied pressure: symbols represent numerical SCF results; solid lines are calculated analytically according to eqs 27, 28, and 6. Brush parameters (chain length N and grafting density σ) are indicated in the legend.

weak function of the external pressure, especially for brushes with relatively high grafting density. (ii) Analytical theory works very well for brushes with low to moderate grafting densities $\sigma \leq 0.1$; some deviations are observed for brushes with $\sigma = 0.3$, although the mismatch between the analytical theory and the numerical SCF results does not exceed 10%; the underlying reason is that eq 3 was derived assuming the second virial approximation for the chemical potential which is not quite accurate for larger monomer densities. (iii) At very low pressures, the analytical theory underestimates the penetration length: the actual brush density profile at the outer edge has a nonparabolic diffuse tail with low slope which is not accounted for by the analytical theory in the strong-stretching approximation but results in an increased penetration length.

A simple approximate solution of eq 28 is available for strong compression

$$\frac{D}{2H_0} \simeq \left(\frac{\pi\sigma}{2} \right)^{2/3} \phi_m^{-1}, \quad \frac{D}{2H_0} \ll 1 \quad (29)$$

which in combination with eq 27 leads to the following expression for the penetration length

$$\begin{aligned} \delta &= B \left(\frac{2}{\pi} \right)^{2/3} 3^{-1/3} \sigma^{-1/3} N^{1/3} (\phi_m(\Pi))^{1/3} \\ &\simeq 0.33 \left(\frac{N}{\sigma} \right)^{1/3} (\phi_m(\Pi))^{1/3} \end{aligned} \quad (30)$$

Hence, we expect the penetration length data for brushes with different chain lengths and grafting densities to collapse onto a single master curve in the coordinates $\delta \left(\frac{\sigma}{N} \right)^{1/3}$ vs Π provided relative compression is relatively large. Figure 8 demonstrates the comparison between the numerical SCF data and the scaling proposed by the approximate analytical theory.

Weak dependence of the penetration length on the pressure as observed in Figure 8 is quite striking. This is related to the range of chain lengths and grafting densities covered by our numerical SCF results. For larger chain lengths N and lower grafting densities σ , the overall range of change in the penetration length increases. However, the analytical theory

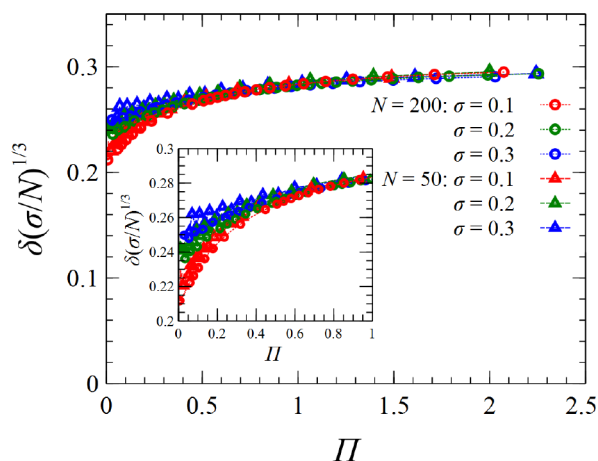


Figure 8. Rescaled penetration length as a function of the applied pressure in the Π ensemble. Brush chain length N and grafting density σ are indicated. (Inset) The same data at small and moderate pressure at a different scale.

suggests that even for $N = 5000$ and $\sigma = 0.01$, the penetration length changes at most by a factor of 2. Hence, a simplified description of the penetration length for monodisperse brushes in the pressure ensemble as a constant is $\delta = C\left(\frac{N}{\sigma}\right)^{1/3}$, where the prefactor $C \approx 0.25$ covers most of the situations of interest. MC simulation results³³ suggest that brush polydispersity may lead only to minor changes in this conclusion.

Figure 9a and 9b displays the interpenetration parameters, namely, the overlap integral $\Gamma(\Pi)$ and surface density of segments beyond the midplane $\Sigma(\Pi)$ obtained by the numerical SCF calculations for several values of the brush parameters N and σ as indicated in the legend. In the lower panels c and d, the data are shown to collapse quite well onto master curves when rescaled by the factor $(\sigma/N)^{1/3}$ according to the simplified analytical result for the penetration length, eq 30. Collapse is not perfect at small pressures, which is due to the behavior of the rescaled penetration length, see previous Figure 8.

We have discussed earlier the ratio of the two interpenetration parameters Γ/Σ and verified that it is proportional to the segment density at the midplane. It follows that in the pressure ensemble the ratio must be a universal function of pressure independent of the brush parameters. The SCF data for Γ/Σ vs pressure are displayed in Figure 10. The inset shows this relation at small pressures where the second virial approximation is valid. According to eqs 4, 12, and 13 we expect

$$\Gamma/\Sigma = \frac{2^{1/2}}{\log 2} \Pi^{1/2} \approx 2.04 \Pi^{1/2} \quad (31)$$

which is consistent with the SCF data.

In the previous section we have demonstrated that the sliding friction force between two brush-coated surfaces in good solvent is expected to be governed by the two integral interpenetration parameters Γ and Σ , see eqs 25 and 26. Expressions for the friction force contain two proportionality

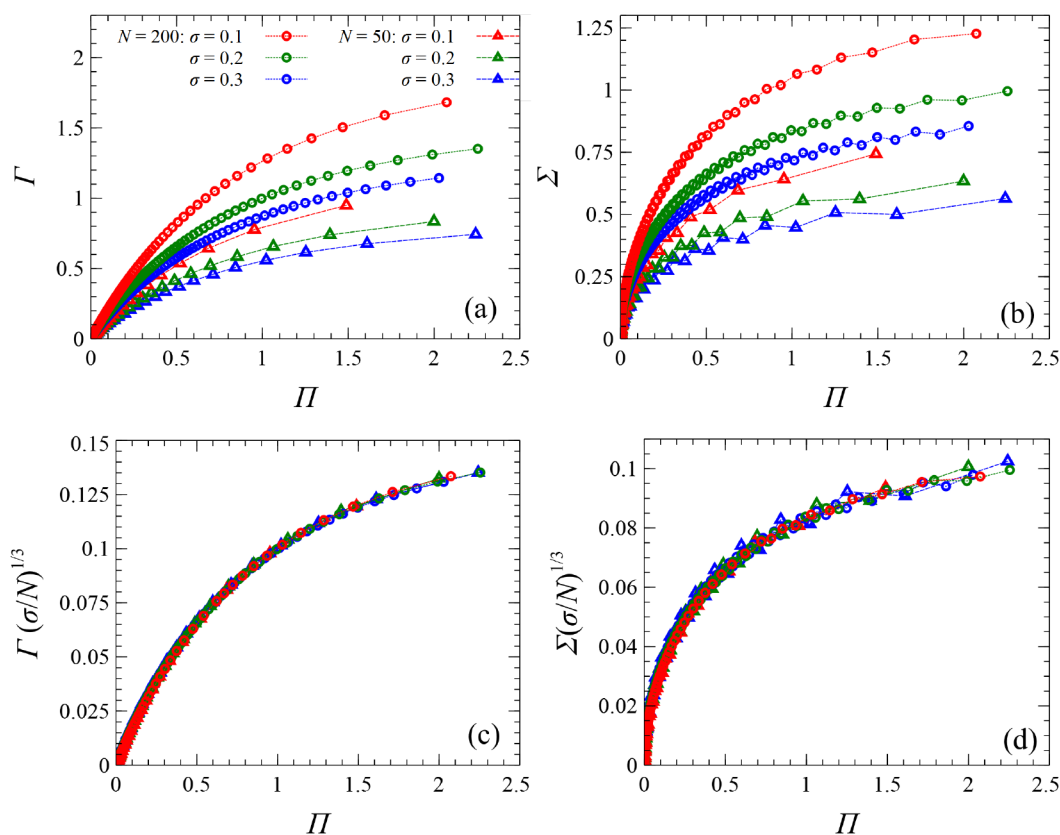


Figure 9. Overlap integral in normal (a) and rescaled (c) form and surface density of monomer units belonging to one of the brushes and residing beyond the midplane in normal (b) and rescaled (d) form as functions of the applied pressure in the Π ensemble. Brush chain length N and grafting density σ are indicated.

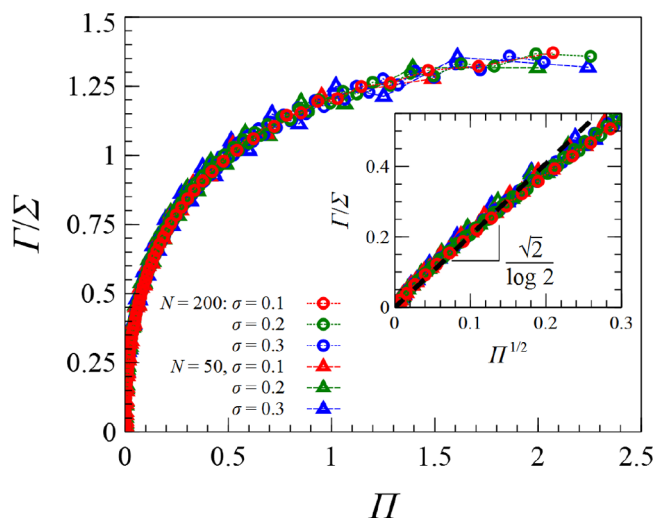


Figure 10. Ratio of the overlap integral Γ and the number of monomer units in foreign region Σ in the Π ensemble. Brush chain length N and grafting density σ are indicated. (Inset) Linear dependence vs $\Pi^{1/2}$ for low pressure.

coefficients ζ_{bb} and ζ_{bs} which have the meaning of the viscous friction coefficient per one brush–brush contact and the segment friction coefficient in the solvent, respectively. In order to simplify the analysis, we take them as equal, $\zeta_{bb} = \zeta_{bs} = \zeta$, which gives

$$F_{\text{fr}} = \left(\frac{\pi + 2}{4} \right) \Gamma \quad (32)$$

for the nondraining limit and

$$F_{\text{fr}} = V\zeta \left[\left(\frac{3}{2} \right) \Gamma + \frac{1}{\ln 2} \Sigma \right] \quad (33)$$

for the free-draining limit. It turns out that the friction force per unit area normalized by the product $V\zeta$ is reduced to the interpenetration parameters and, hence, is expected to be described by universal functions of the applied pressure after rescaling by the factor of $\left(\frac{\sigma}{N} \right)^{1/3}$. Figure 11a displays the appropriate combinations of the integral interpenetration parameters representing the normalized and rescaled friction

force $\frac{F_{\text{fr}}}{V\zeta} \left(\frac{\sigma}{N} \right)^{1/3}$ vs the applied pressure, Π , for the nondraining and the free draining limits.

Dry friction produced by a sliding motion of two surfaces against each other is traditionally described by the kinetic friction coefficient as the ratio of the friction force to the loading force normal to the moving surface. We apply the same definition with both forces evaluated per unit area, $\mu = \frac{F_{\text{fr}}}{\Pi}$. Note that in contrast to dry friction, which is almost independent of the relative velocity, we are dealing with viscous friction in the low Weissenberg number limit when the force is linear in the sliding velocity. Panel b of Figure 11 displays the normalized and rescaled friction coefficient $\frac{\mu}{V\zeta} \left(\frac{\sigma}{N} \right)^{1/3}$ as a function of the applied pressure (note that the pressure is expressed in units of $k_B T/a^3$, which is omitted in Figure 11). The universal behavior of the friction force in the pressure ensemble naturally leads to the same universality for the friction coefficient μ .

Two features can be observed very clearly. First, the free-draining limit generally corresponds to larger friction forces than the nondraining limit, which is to be expected. Second, the friction coefficient is a decreasing function of pressure. In the nondraining limit controlled by the overlap integral Γ , this is due to higher virial terms in the equation of state. In the free-draining limit, the change in the friction coefficient with pressure is more dramatic: one contribution to the friction force comes from the number of segments in the foreign half-space, Σ , which is proportional to the segment density at the midplane, φ_m , and therefore scales as $\Sigma \approx \Pi^{1/2}$ at low pressures (second virial regime). This naturally leads to a divergence of the friction coefficient $\mu \approx \Pi^{-1/2}$ at low pressures. In contrast, in the nondraining limit, the friction coefficient μ remains finite at low pressures. A note of caution is due at this point since the estimate of the contribution to friction due to induced solvent motion was made under the assumption that the penetration length δ is considerably larger than the hydrodynamic screening length. This assumption may be not valid at very low pressures when the segment density in the interpenetration zone is also low, leading to a relatively large hydrodynamic length. Hence, our results based on the approximate treatment

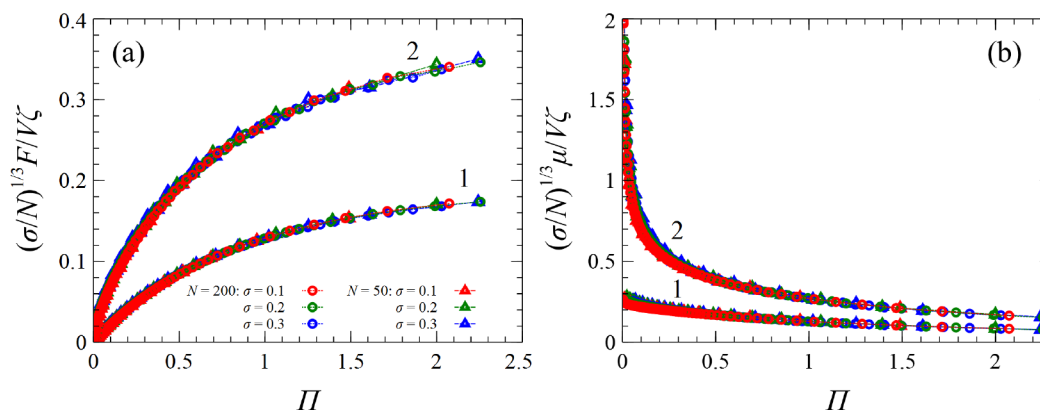


Figure 11. Normalized and rescaled friction force (a) and the corresponding normalized and rescaled friction coefficient (b) as functions of the applied pressure for the sliding motion of two brush-coated surfaces against each other in the pressure ensemble. See the text for explanation. Master curves labeled 1 describe the nondraining limit; master curves labeled 2 describe the free-draining limit. Chain length N and grafting density σ are indicated in the legend of panel a.

of the Brinkman equation in the low-pressure regime are preliminary, and a more careful consideration is required.

4. SUMMARY AND OUTLOOK

The main focus of the present paper was to establish a relation between the external normal pressure applied to two opposing monodisperse brushes and the lateral friction forces generated by shearing. We identify the pressure due to external load with the osmotic pressure since in a typical experimental situation the solvent permeating the brushes is connected to a reservoir usually exposed to atmospheric pressure. The same atmospheric pressure is transmitted to the exterior of the brush-coated surfaces so that in the absence of external load mechanical equilibrium is achieved without any extra repulsion between brushes. A different approach was taken in the work by Goujon et al.,^{24,25} where DPD simulations included pressure due to explicit solvent. The solvent pressure was by far dominating the osmotic brush contribution, and hence, the total pressure was changing only very weakly as a function of the brush separation. This leads to a different behavior of the friction coefficient defined as the ratio of the sliding friction force to the total (rather than osmotic) pressure.

We have several reasons to promote the use of the pressure (Π) ensemble as opposed to the brush separation (D) ensemble in order to rationalize the brush interpenetration. First, external pressure seems a more natural variable to operate with under experimental conditions. Accurate control of the brush separation is quite difficult even for special surface force apparatus, while controlling the external load is more versatile. In the context of brushes found in living organisms or brushes used in prosthetic joints, the D ensemble looks particularly artificial.

Second, the pressure ensemble provides a natural setting for comparing the tribological properties of brushes differing in terms of the chain length, grafting density, polydispersity, or chemical composition. This comparison should be based on the friction coefficient function $\mu(\Pi)$.

Third, the behavior of the tribological properties of compressed brushes turns out to be quite universal in the pressure ensemble, at least for monodisperse brushes in good solvent that we were concerned with in the present paper.

We have shown that two integral interpenetration characteristics Γ (number of brush–brush contacts) and Σ (number of segments in the foreign half-space) control the sliding friction forces. Their universal behavior in the pressure ensemble stems from the fact that they are completely defined by the segment density at the midplane, φ_m , and the penetration length, δ . The former is a function of pressure only (through the equation of state for a semidilute solution) independent of the brush parameters, while the latter is reasonably described as a pressure-independent quantity that contains all of the information about the brush and in the case of monodisperse brushes scales as $\delta \approx \left(\frac{N}{\sigma}\right)^{1/3}$.

As a consequence, we were able to demonstrate that the ratio of the two integral interpenetration characteristics Γ/Σ is a linear function of the midplane density independent of the brush parameters and, therefore, a universal function of pressure. We predict this result to be insensitive to the brush polydispersity as well.

Yet, another consequence is the universality of the rescaled interpenetration characteristics $(\sigma/N)^{1/3}\Gamma$ and $(\sigma/N)^{1/3}\Sigma$ in the pressure ensemble.

We should note that although in our calculations we have used the Flory–Huggins equation of state (historically, it was built into the Scheutjens–Fleer self-consistent field lattice algorithm we employed), our main conclusions are quite insensitive to this specific choice. Other forms of the equation of state have been used to describe polymer–polymer interactions. In particular, versions of the Carnahan–Starling equation of state were shown to be in good agreement with the results of MD simulations⁴⁰ and employed in several studies involving dense brushes.^{41–43} A new universal equation of state for flexible polymers was proposed recently in ref 44 and tested in a wide range of polymer concentrations against MD simulations and experimental data. However, the universal behavior of the tribological properties of brushes found in the present work is based on eqs 12, 13, and 30 and relies only on the natural assumption that *some* equation of state relating the polymer density at the midplane to the brush osmotic pressure does exist.

We have based our narrative concerning the interpenetration parameters and their connection to the sliding friction forces on a simple picture of viscous friction due to monomer–monomer and monomer–solvent relative motion. It is natural to question the possible role of chain entanglements since they can greatly enhance the observed viscosity. Clearly, the equilibrium SCF method is not suited to address this question. Conformations with intrabrush entanglements have been studied in ref 45 by MD, while entanglement effects on the brush chain dynamics were observed in ref 46 and thoroughly analyzed in ref 47. It is important to distinguish between intrabrush and interbrush entanglements since only the latter may potentially affect the sliding friction forces. Goujon et al.⁴⁸ attempted to quantify the effect of entanglements for a two-brush system in a DPD simulation, but it was difficult to separate explicitly the effects that are due to additional repulsive interactions and those associated with proper disentanglement dynamics. Indirect estimates can be drawn from the intrabrush entanglement studies. A detailed analysis by Lang et al.⁴⁷ concludes that chain dynamics in a dense monodisperse brush is controlled by a retraction mechanism that leads to exponentially large relaxation times $\tau \approx N^3 \exp(N/N_e)$ with the characteristic entanglement length $N_e \approx 6g$, where g is the number of monomers in the concentration blob. If applied literally to the interpenetration zone, one would expect entanglement effects to be quite prominent under the conditions $\delta^2 \gtrsim N_e$. At strong compressions $g \approx 1$, this condition is already satisfied for the brush parameters studied above with the penetration lengths in the range of $2 \lesssim \delta \lesssim 4$ and even more so for larger N and smaller grafting densities. It is important to note though that since the interpenetration zone contains only relatively small end portions of the brush chains, the entanglement release is not limited to the retraction mechanism: brush chain fluctuations within the entanglement tube may provide a faster release mechanism. Overall, the tentative role of chain entanglements in defining the sliding friction remains an open question and calls for further investigations.

Let us finally recall that the unit pressure $\Pi = 1$ in SCF calculations and analytical theory is approximately equal to 40 atm; hence, the applied pressure of 1 atm (the most common everyday value) corresponds to $\Pi = 0.025$ in SCF calculations. Note also that the pressure range up to 5 atm is well described by the equation of state in the second virial approximation.

■ ASSOCIATED CONTENT

SI Supporting Information

The Supporting Information is available free of charge at <https://pubs.acs.org/doi/10.1021/acs.macromol.3c00458>.

Calculation of the solvent velocity profile and the resulting friction forces mediated by the solvent flow for two opposing interpenetrating brushes immersed in good solvent and sliding against each other (PDF)

■ AUTHOR INFORMATION

Corresponding Author

Leonid I. Klushin – *Institute of Macromolecular Compounds,, Russian Academy of Sciences, Saint Petersburg 199004, Russia; Department of Physics, American University of Beirut, Beirut 1107 2020, Lebanon; Email: leo@aub.edu.lb*

Authors

Anna S. Ivanova – *Institute of Macromolecular Compounds,, Russian Academy of Sciences, Saint Petersburg 199004, Russia*

Alexey A. Polotsky – *Institute of Macromolecular Compounds,, Russian Academy of Sciences, Saint Petersburg 199004, Russia; orcid.org/0000-0002-3286-1652*

Alexander M. Skvortsov – *Chemical-Pharmaceutical University, St. Petersburg 197022, Russia*

Complete contact information is available at:

<https://pubs.acs.org/doi/10.1021/acs.macromol.3c00458>

Notes

The authors declare no competing financial interest.

■ ACKNOWLEDGMENTS

Financial support by the Russian Foundation for Basic Research through Grant 20-53-12020 NNIO_a is gratefully acknowledged.

■ REFERENCES

- (1) Ayres, N. Polymer brushes: Applications in biomaterials and nanotechnology. *Polym. Chem.* **2010**, *1*, 769–777.
- (2) Motornov, M.; Minko, S.; Eichhorn, K.-J.; Nitschke, M.; Simon, F.; Stamm, M. Reversible tuning of wetting behavior of polymer surface with responsive polymer brushes. *Langmuir* **2003**, *19* (19), 8077–8085.
- (3) Urban, M. W. *Handbook of Stimuli-Responsive Materials*; Wiley-VCH Verlag GmbH & Co. KGaA: Weinheim, Germany, 2011.
- (4) Klein, J.; Perahia, D.; Warburg, S. Forces between polymer-bearing surfaces undergoing shear. *Nature* **1991**, *352*, 143–145.
- (5) Klein, J. Shear, friction, and lubrication forces between polymer-bearing surfaces. *Annu. Rev. Mater. Sci.* **1996**, *26* (1), 581–612.
- (6) Klein, J. Repair or replacement—a joint perspective. *Science* **2009**, *323* (5910), 47–48.
- (7) Taunton, H. J.; Toprakcioglu, C.; Fetters, L. J.; Klein, J. Interactions between surfaces bearing end-adsorbed chains in a good solvent. *Macromolecules* **1990**, *23* (2), 571–580.
- (8) Pelletier, E.; Stamouli, A.; Belder, G. F.; Hadziioannou, G. Adsorption kinetics of an asymmetric diblock copolymer: A surface forces apparatus study. *Langmuir* **1997**, *13* (7), 1884–1886.
- (9) Drobek, T.; Spencer, N. D.; Heuberger, M. Compressing PEG Brushes. *Macromolecules* **2005**, *38* (12), 5254–5259.
- (10) Milner, S. T. Hydrodynamic penetration into parabolic brushes. *Macromolecules* **1991**, *24* (12), 3704–3705.
- (11) Milner, S. T. Compressing polymer “brushes”: a quantitative comparison of theory and experiment. *Eur. Phys. Lett.* **1988**, *7* (8), 695–699.
- (12) Qi, S.; Klushin, L. I.; Skvortsov, A. M.; Schmid, F. Polydisperse polymer brush: Internal structure, critical behavior, and interaction with flow. *Macromolecules* **2016**, *49*, 9665–9683.
- (13) Wijmans, C. M.; Zhulina, E. B.; Fleer, G. J. Effect of free polymer on the structure of a polymer brush and interaction between two polymer brushes. *Macromolecules* **1994**, *27* (12), 3238–3248.
- (14) Galuschko, A.; Spirin, L.; Kreer, T.; Johner, A.; Pastorino, C.; Wittmer, J.; Baschnagel, J. Frictional forces between strongly compressed, nonentangled polymer brushes: Molecular dynamics simulations and scaling theory. *Langmuir* **2010**, *26* (9), 6418–6429.
- (15) Singh, M. K.; Ilg, P.; Espinosa-Marzal, R. M.; Kröger, M.; Spencer, N. D. Polymer brushes under shear: Molecular dynamics simulations compared to experiments. *Langmuir* **2015**, *31* (16), 4798–4805.
- (16) Doyle, P. S.; Shaqfeh, E. S. G.; Gast, A. P. Rheology of polymer brushes: A brownian dynamics study. *Macromolecules* **1998**, *31* (16), 5474–5486.
- (17) Kreer, T.; Müser, M. H.; Binder, K.; Klein, J. Frictional drag mechanisms between polymer-bearing surfaces. *Langmuir* **2001**, *17* (25), 7804–7813.
- (18) Kreer, T.; Binder, K.; Müser, M. H. Friction between polymer brushes in good solvent conditions: Steady-state sliding versus transient behavior. *Langmuir* **2003**, *19* (18), 7551–7559.
- (19) Kreer, T. Polymer-brush lubrication: a review of recent theoretical advances. *Soft Matter* **2016**, *12*, 3479–3501.
- (20) Chakrabarti, A.; Nelson, P.; Toral, R. Interpenetrations in polymer brushes. *J. Chem. Phys.* **1994**, *100* (1), 748–749.
- (21) Grest, G. S. Interfacial sliding of polymer brushes: A molecular dynamics simulation. *Phys. Rev. Lett.* **1996**, *76* (Jun), 4979–4982.
- (22) Elliott, I. G.; Kuhl, T. L.; Faller, R. Compression of high grafting density opposing polymer brushes using molecular dynamics simulations in explicit solvent. *J. Phys. Chem. B* **2013**, *117* (15), 4134–4141.
- (23) Spirin, L.; Galuschko, A.; Kreer, T.; Johner, A.; Baschnagel, J.; Binder, K. Polymer-brush lubrication in the limit of strong compression. *Eur. Phys. J. E* **2010**, *33* (4), 307–311.
- (24) Goujon, F.; Ghoufi, A.; Malfreyt, P.; Tildesley, D. J. Frictional forces in polyelectrolyte brushes: effects of sliding velocity, solvent quality and salt. *Soft Matter* **2012**, *8*, 4635–4644.
- (25) Goujon, F.; Ghoufi, A.; Malfreyt, P.; Tildesley, D. J. The kinetic friction coefficient of neutral and charged polymer brushes. *Soft Matter* **2013**, *9*, 2966–2972.
- (26) Fleer, G. J.; Cohen Stuart, M. A.; Scheutjens, J. M. H. M.; Cosgrove, T.; Vincent, B. *Polymers at Interfaces*; Chapman and Hall: London, 1993.
- (27) Wijmans, C. M.; Scheutjens, J. M. H. M.; Zhulina, E. B. Self-consistent field theories for polymer brushes: lattice calculations and an asymptotic analytical description. *Macromolecules* **1992**, *25* (10), 2657–2665.
- (28) de Vos, W. M.; Leermakers, F. A. M. Modeling the structure of a polydisperse polymer brush. *Polymer* **2009**, *50* (1), 305–316.
- (29) Ivanova, A. S.; Polotsky, A. A.; Skvortsov, A. M.; Klushin, L. I.; Schmid, F. Adsorption-active polydisperse brush with tunable molecular mass distribution. *J. Chem. Phys.* **2022**, *156* (4), 044902.
- (30) Alexander, S. Adsorption of Chain Molecules with a Polar Head: A Scaling Description. *J. Phys. (Paris)* **1977**, *38* (8), 983–987.
- (31) de Gennes, P.-G. Conformations of Polymers Attached to an Interface. *Macromolecules* **1980**, *13* (5), 1069–1075.
- (32) Milner, S. T.; Witten, T. A.; Cates, M. E. Theory of the grafted polymer brush. *Macromolecules* **1988**, *21* (8), 2610–2619.
- (33) Klushin, L. I.; Skvortsov, A. M.; Qi, S.; Kreer, T.; Schmid, F. Polydispersity effects on interpenetration in compressed brushes. *Macromolecules* **2019**, *52* (4), 1810–1820.
- (34) Murat, M.; Grest, G. S. Interaction between grafted polymeric brushes: A molecular-dynamics study. *Phys. Rev. Lett.* **1989**, *63* (Sep), 1074–1077.
- (35) Witten, T. A.; Leibler, L.; Pincus, P. A. Stress relaxation in the lamellar copolymer mesophase. *Macromolecules* **1990**, *23* (3), 824–829.

- (36) Erbas, A.; Paturej, J. Friction between ring polymer brushes. *Soft Matter* **2015**, *11*, 3139.
- (37) Brinkman, H. C. A calculation of the viscous forces exerted by a flowing fluid on a dense swarm of particles. *Appl. Sci. Res.* **1949**, *1*, 27–34.
- (38) Suo, T.; Whitmore, M. D. Doubly self-consistent field theory of grafted polymers under simple shear in steady state. *J. Chem. Phys.* **2014**, *140* (11), 114901.
- (39) Wijmans, C. M.; Smit, B. Simulating tethered polymer layers in shear flow with the dissipative particle dynamics technique. *Macromolecules* **2002**, *35* (18), 7138–7148.
- (40) Romeis, D.; Merlitz, H.; Sommer, J.-U. A new numerical approach to dense polymer brushes and surface instabilities. *J. Chem. Phys.* **2012**, *136* (4), 044903.
- (41) Merlitz, H.; Cui, W.; Wu, C.-X.; Sommer, J.-U. Semianalytical Mean-Field Model for Starlike Polymer Brushes in Good Solvent. *Macromolecules* **2013**, *46*, 1248–1252.
- (42) de Vos, W. M.; Biesheuvel, P. M.; de Keizer, A.; Kleijn, J. M.; Cohen Stuart, M. A. Adsorption of the protein bovine serum albumin in a planar poly(acrylic acid) brush layer as measured by optical reflectometry. *Langmuir* **2008**, *24* (13), 6575–6584.
- (43) de Vos, W. M.; Biesheuvel, P. M.; de Keizer, A.; Kleijn, J. M.; Cohen Stuart, M. A. Adsorption of anionic surfactants in a nonionic polymer brush: Experiments, comparison with mean-field theory, and implications for brush-particle interaction. *Langmuir* **2009**, *25* (16), 9252–9261.
- (44) Paturej, J.; Sommer, J.-U.; Kreer, T. Universal equation of state for flexible polymers beyond the semidilute regime. *Phys. Rev. Lett.* **2019**, *122* (Feb), 087801.
- (45) Hoy, R. S.; Grest, G. S. Entanglements of an End-Grafted Polymer Brush in a Polymeric Matrix. *Macromolecules* **2007**, *40* (23), 8389–8395.
- (46) Reith, D.; Milchev, A.; Virnau, P.; Binder, K. Computer simulation studies of chain dynamics in polymer brushes. *Macromolecules* **2012**, *45* (10), 4381–4393.
- (47) Lang, M.; Werner, M.; Dockhorn, R.; Kreer, T. Arm Retraction Dynamics in Dense Polymer Brushes. *Macromolecules* **2016**, *49* (14), 5190–5201.
- (48) Goujon, F.; Malfreyt, P.; Tildesley, D. J. Mesoscopic simulation of entanglements using dissipative particle dynamics: Application to polymer brushes. *J. Chem. Phys.* **2008**, *129* (3), 034902.